Modeling In-Situ SiO_2 Particle Deposition for Thermal Barrier Coatings in Rocket-Like Flows

William Dugan

August 2, 2025

Abstract

This project investigates the modeling of SiO_2 particle-laden flows relevant to thermal barrier coating (TBC) deposition in rocket-like environments. The gas-phase flow is modeled as a steady, incompressible, fully developed channel flow, serving as a simplified analog for high-temperature internal flows encountered in propulsion systems. Turbulence is addressed using Reynolds-Averaged Navier–Stokes (RANS) equations with eddy viscosity models, including Prandtl's mixing-length approach and near-wall treatments.

Building on the computed mean velocity field, the Lagrangian dynamics of heavy, inertial SiO_2 particles are simulated under the assumption of one-way coupling and low particle Reynolds numbers. Particle motion is governed by a simplified Basset–Boussinesq–Oseen (BBO) equation, incorporating Stokes drag and interpolated gas-phase velocities. The goal is to understand particle behavior near walls, which directly impacts deposition patterns and coating efficiency.

In many rocket engines, film cooling is used by injecting additional fuel along the wall to shield it from the hot core flow. This alters the overall gas flow field and introduces a second gas or vapor phase, effectively creating a multi-component system. Although film cooling is not included in the current simulations, the framework is designed to support it. The numerical setup can incorporate externally provided flow profiles, enabling future studies on how film cooling affects particle dynamics and wall deposition.

IMPORTANT NOTE: The results presented here are different from the results in the presentation from 10.07.2025 - an issue with face interpolation of viscosity has been fixed after the presentation.

Contents

1 Introduction

1.1 Motivation

Internal combustion engines generate gas flows with temperatures often exceeding the maximum allowable temperature of the containing structure. A wide variety of cooling methods exist to address this challenge, all of which operate by one or both of the following principles: (a) reducing heat transfer from the gas to the structure, and (b) enhancing heat dissipation from the structure to an external medium — effectively reducing heat intake or increasing heat output. This project focuses on the first principle, specifically the use of thermal barrier coatings (TBCs) in rocket engines. While the findings are targeted at rocket engines, they may also be applicable to other internal combustion engines when combined with additional cooling techniques.

TBCs reduce heat transfer by increasing the thermal resistance between the hot combustion gases and the engine's structural wall. In rocket engine cooling systems, several thermal resistances act in series, as illustrated in Figure 1. Typically, TBCs exhibit low thermal conductivity—on the order of 1 W/mK—which enables them to effectively insulate the engine structure from the extreme combustion temperatures. Due to the high heat fluxes in rocket engines, TBCs must be relatively thin; excessively thick coatings lead to large temperature gradients across the layer, inducing thermal stresses that can cause cracking or delamination. The typical thickness of TBCs ranges from approximately 1 µm to 1 mm.

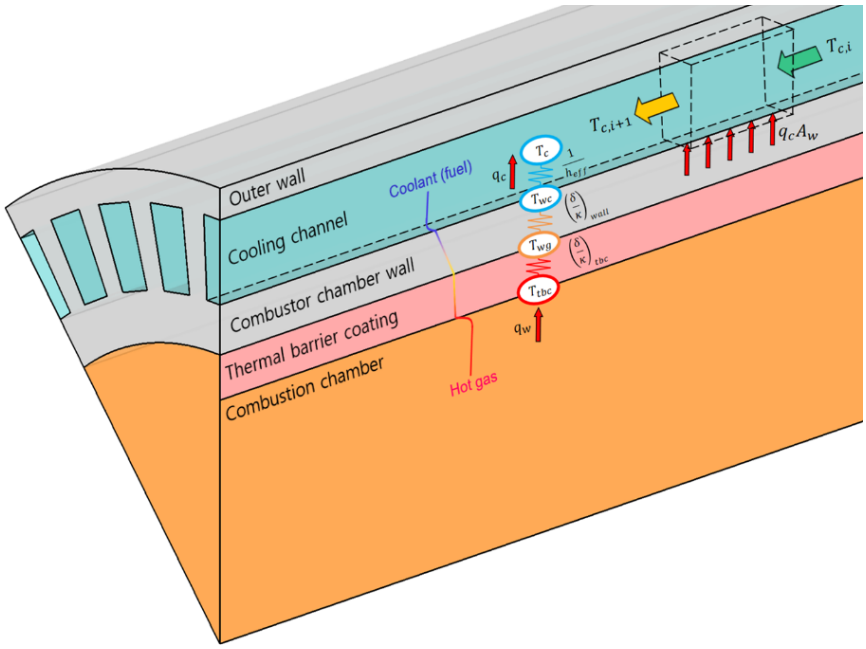

Figure 1: A typical thermal resistance system in a rocket engine cooling system. [1]

Thermal barrier coatings in student-developed rocket engines are often applied in situ,

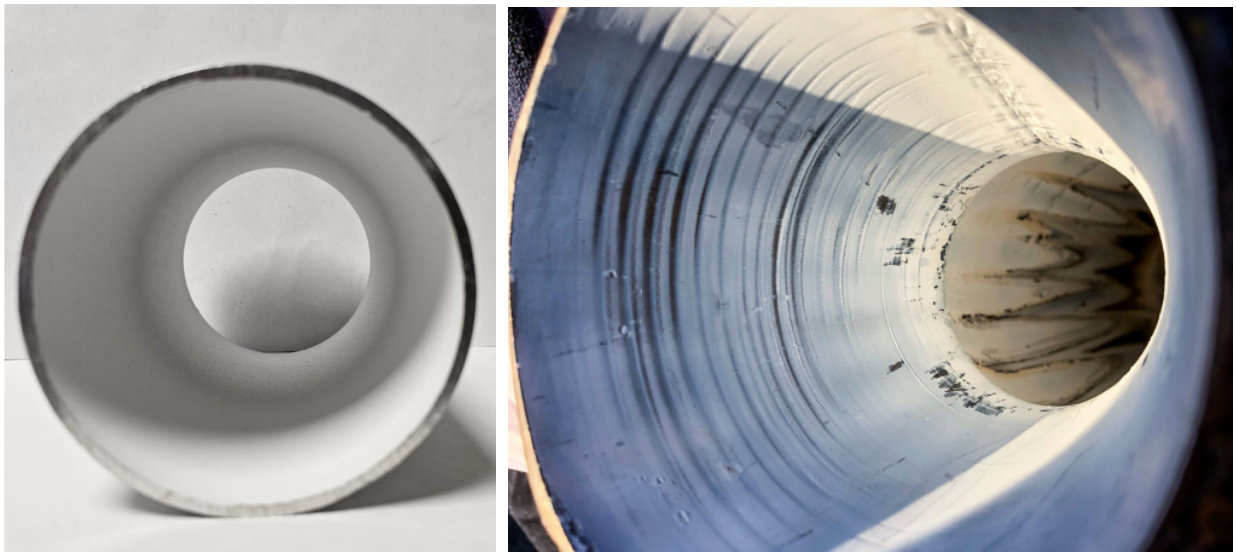

(a) Example of a TBC configuration dissimilar to the one used in this study. A 200 µm to 500 µm layer of ThermoHold® H2000, a zirconia-based ceramic coating, is applied via atmospheric plasma spraying over a 50 µm nickel-based bond coat [2].

(b) Example of a TBC configuration closely resembling the one used in this study. A fine layer of silicon dioxide (SiO_2) is formed in situ by combusting a fuel blend containing tetraethyl orthosilicate (TEOS), as demonstrated in [3]. The visible streak patterns (right) are a result of the discrete injection points in the injector, which features a finite number of orifices rather than a continuous distribution.

Figure 2: Examples of TBC configurations used in related studies.

for example by combusting fuel blends containing TEOS, PDMS or silicone oil, resulting in coatings that form during engine operation. This method tends to produce coatings with irregular thickness and non-uniform surface features due to localized deposition influenced by the injector geometry and flow conditions, as shown in Figure 2b. Due to the dynamic nature of this deposition, the actual coating thickness and uniformity are difficult to quantify precisely. Consequently, many studies and simulations simply assume a reasonable or nominal TBC thickness, possibly introducing significant uncertainty in thermal protection predictions.

In addition to the uncertainties associated with in-situ TBC formation, the use of film cooling in rocket engines introduces further complexity. Film cooling involves injecting fluid (often gaseous or liquid fuel) along the chamber walls to protect the structure, but this creates highly variable temperature and flow conditions near the surface. These variations significantly affect particle deposition patterns and thermal gradients, making it difficult to predict how the TBC will develop and perform in practice. Since film cooling modifies both the heat transfer and coating formation environment, it adds another layer of uncertainty that has yet to be fully characterized or integrated into most models.

1.2 Assumptions and simplifications

Most rocket engines reach steady-state operation within a few seconds after ignition. For this project, the analysis is limited to steady-state conditions, simplifying the flow simulation by neglecting transient effects. Although the particles involved in the deposition process are in motion, their time-dependent behaviour is modeled using a quasi-1D approach, which decouples time progression and spatial movement. This approximation assumes that gas flow and particle behaviour can be described primarily along one spatial dimension, significantly reducing computational complexity. It works well for the core flow in a rocket engine but is less accurate near the wall regions and close to the throat, where multi-dimensional effects and complex flow phenomena such as compressibility, shock formation, and dissociation become significant.

Rocket engines typically feature a cylindrical-converging-diverging nozzle geometry and are axisymmetric by design. To reduce computational effort, this study focuses only on the cylindrical section of the nozzle. Furthermore, to avoid complications associated with cylindrical coordinates, the geometry is simplified to a two-dimensional channel flow. By assuming an infinitely large span-wise dimension, the problem reduces effectively to one dimension.

Modeling combustion directly is inherently complex and falls outside the scope of this project. Instead, it is assumed that the combustion gas properties are known and constant. Under these assumptions, gas properties are approximated using precomputed equilibrium results from tools such as NASA CEA or Cantera.

The particle tracking employs a one-way coupling approach, where the particles do not affect the gas flow. Particles are represented as parcels, each corresponding to approximately 1000 identical particles. Their motion is assumed to be governed by Stokes drag. Effects such as particle-particle interactions, agglomeration, or break-up are neglected, simplifying the deposition modeling but potentially reducing accuracy in regions of high particle concentration or turbulence.

1.3 Problem statement

This project investigates the wall-deposition behaviour of particles used for in-situ TBCs in rocket engines. Using a highly simplified, quasi-one-dimensional statistical steady-state channel flow model with one-way coupled Lagrangian particle tracking, the goal is to estimate the resulting TBC thickness along the wall. The analysis assumes known combustion gas properties, neglects combustion dynamics, and uses representative particle parcels governed by Stokes drag. While the simplified geometry and assumptions limit direct applicability to full engine designs, the model serves as a foundational step toward understanding deposition behaviour — especially in cases where film cooling and in-situ coatings interact in poorly understood ways.

2 Theory

2.1 Single-Phase Channel Flow

The gas-phase flow in this study is modelled as a steady, incompressible, single-phase flow in a simplified channel geometry. Specifically, assume fully developed, one-dimensional channel flow under steady-state and incompressible conditions.

2.1.1 Transport Equations

For a steady channel flow with constant density and viscosity, continuity and momentum conservation reduce to

$$\begin{cases} 0 = \mu \frac{\partial^2 u}{\partial y^2} - \frac{\partial p}{\partial x}, & 0 < y < H \\ u = 0 & y = 0, H \end{cases} \tag{1}$$

where $u = u(y)$. The analytical solution to (1) is

$$u = \frac{1}{2\mu} \frac{\partial p}{\partial x} (y^2 - yH) \tag{2}$$

This is the flow field for Poiseuille flow and exists only for constant viscosity. If the flow becomes turbulent, the viscosity is no longer constant in the y-direction. The problem may be rewritten as

$$\begin{cases} 0 = \frac{\partial}{\partial y}\left(\mu(y) \frac{\partial u}{\partial y}\right) - \frac{\partial p}{\partial x}, & 0 < y < H \\ u = 0 & y = 0, H \end{cases} \tag{3}$$

Note that $\mu = \mu(y)$ in this case. Equation 3 may be solved using a finite volume approach. The system is linear if $\mu(y)$ is known. A more common situation is $\mu = \mu(u(y))$, making the system non-linear. The solution can be obtained by solving a linear system iteratively and updating the viscosity profile between each iteration. See 3.2 for more information.

2.1.2 Reynolds Averaging

Turbulent flow is commonly modelled using Reynolds-averaged Navier–Stokes (RANS) equations. The velocity is decomposed into a mean and a fluctuating component, $u = U + u'$, where $U = \overline{u}$ is the time-averaged velocity and u' is the fluctuating part. One can show that by inserting this decomposition into the momentum equation, applying time-averaging and continuity of both U and u', the RANS equation is

$$\begin{cases} 0 = \frac{\partial}{\partial y}\left(\mu(y) \frac{\partial U}{\partial y} - \rho \overline{u'v'}\right) - \frac{\partial p}{\partial x}, & 0 < y < H \\ U = 0 & y = 0, H \end{cases} \tag{4}$$

Here, $\overline{u'v'}$ is the Reynolds stress, which introduces a closure problem since it depends on unknown fluctuating quantities. To close the system, a turbulence model is required. Under

the Boussinesq approximation, turbulence effects are captured by modifying the effective viscosity. The total viscosity is given by:

$$\mu = \mu_{\text{mol}} + \mu_t \tag{5}$$

where μ_{mol} is the molecular viscosity and μ_t is the turbulent (or eddy) viscosity. The Reynolds stress tensor becomes:

$$\rho\overline{u_j' u_i'} = \frac{2}{3}\rho k\delta_{ij} - 2\mu_t\left(S_{ij} + \frac{1}{3}S_{kk}\delta_{ij}\right) \tag{6}$$

where S_{ij} is the strain rate tensor. Due to continuity, $S_{kk} = 0$. Substituting into the momentum equation yields the final form of the RANS equation:

$$\begin{cases} 0 = \frac{\partial}{\partial y}\left[(\mu_{\text{mol}} + \mu_t(y))\frac{\partial U}{\partial y}\right] - \frac{\partial p}{\partial x}, & 0 < y < H \\ U = 0 & y = 0, H \end{cases} \tag{7}$$

Once the turbulent viscosity profile $\mu_t(y)$ is determined from a chosen model, the velocity profile can be computed using the same numerical method as in the laminar case.

2.1.3 Scales of Turbulence

Three fundamental turbulent scales are commonly defined:

- **Velocity scale, u':** A characteristic magnitude of the velocity fluctuations.
- **Length scale, l:** Representative size of the energy-containing eddies responsible for turbulent transport.
- **Time scale, T_t:** The turnover or lifetime of the turbulent eddies, often related as $T_t = l/u'$.

These scales can be combined to form the turbulent (or eddy) viscosity, which models the enhanced momentum diffusion due to turbulence:

$$\nu_t \sim u' l \tag{8}$$

The turbulent viscosity is generally much larger than the molecular viscosity in fully turbulent regions.

Several turbulence models have been developed based on these scales. The simplest and historically significant model is the Prandtl mixing length model, which estimates turbulent viscosity using a spatially varying mixing length and the local velocity gradient.

More advanced two-equation models, such as the k-ε model, solve transport equations for turbulent kinetic energy (k) and its dissipation rate (ε), providing a more robust and general prediction of turbulence effects in complex flows. [4]

2.1.4 Mixing Length Models

The simplest turbulence model is the Prandtl mixing length model with length scale $l \sim l_m$ and velocity scale $u' \sim l_m dU/dy$, yielding

$$\nu_t = l_m^2 \left| \frac{dU}{dy} \right| \tag{9}$$

Here, l_m is a mixing length representing the size of the eddies, and dU/dy is the velocity gradient for the mean flow. Eddies in wall-bounded flows must naturally decrease in size when approaching the wall. This implies that $l_m = f(y)$ and that $l_m(y \to 0) = 0$. For wall-bounded flow, one may use [4]

$$l_m = \begin{cases} \kappa y, & y < C\delta \\ \kappa C\delta & \text{otherwise} \end{cases} \tag{10}$$

where $\kappa \approx 0.4$ is the von Kármán constant, and δ is the boundary layer thickness. For a steady flow in a channel of height H, the boundary layer height is $\delta = H/2$. Experiments show that $C = 0.09$ for flow over a flat plate, and $C \approx 0.19$ for a channel flow. [4] The latter is used for the remainder of this project. Note that y in (10) is the distance to the closest wall, i.e. $y = \min(y, H - y)$ for a channel centred around $H/2$.

2.1.5 Eddy viscosity models

$k - \varepsilon$ etc. Not implemented due to time constraints.

2.1.6 Wall treatment

Wall treatment is essential in turbulence modeling because the flow behaviour near the wall differs significantly from the core flow, featuring steep velocity gradients and viscous effects. Accurate representation of this near-wall region is critical for predicting shear stresses, heat transfer, and particle deposition.

The distance to the closest wall in so-called wall units is

$$y^+ = \frac{y u_\tau}{\nu} \tag{11}$$

where y is the distance from the cell center to the nearest wall, ν is the (molecular) kinematic viscosity, and the friction velocity u_τ is defined as

$$\rho u_\tau^2 = \tau_w \tag{12}$$

where τ_w is the shear stress at the wall. Using y^+ it is possible to derive two different cases which need to be handled differently, in addition to one case which should be avoided:

- $\mathbf{y^+ < 1}$: A good well-resolved mesh will have a y^+ value approximately less than one. It is required to dampen the turbulence effects close to the wall. A common

technique is to use van Driest damping, which is a multiplicative correction to the provided mixing length $l_m(y)$:

$$f(y^+) = 1.0 - e^{-y^+/A^+} \tag{13}$$

$$l_m^*(y, y^+) = l_m(y) f(y^+) \tag{14}$$

where $A^+ = 26$. The damping function is applied to the whole channel.

- $\mathbf{30 < y^+ < 300}$: A good wall-function mesh will have a y^+ value inside the so-called log-law region. The velocity profile is derived from boundary layer theory and is provided as an implicit relation known as the law of the wall. Together with the boundary conditions, the law of the wall will provide the velocity for the first internal cell. The dimensionless wall velocity is

$$u^+ = \frac{u}{u_\tau} \tag{15}$$

and the law of the wall is

$$u^+ = \frac{1}{\kappa} \log(y^+) + B \tag{16}$$

There are many versions of this function, and here the constant $B = 5$ is used. Surface roughness is not considered here, but it is possible to alter the law of the wall to include roughness effects.

- $\mathbf{5 < y^+ < 30}$: The buffer layer is located between the two aforementioned regions and should be avoided.

For all the regions above, it is clear that the first cell center cannot be placed *at* the wall, but somewhere close to it. Re-meshing is sometimes necessary since y^+ is not known a-priori.

2.2 Particle-laden channel flow

2.2.1 Equation of motion

Consider heavy particles dispersed in a thin gas, $\rho_p/\rho >> 1$ with one-way coupling. For this case, Stokes drag can be considered as the only significant body force on the particle, since the particle Reynolds number is low, $Re_p = D_p|u - v_p|/\nu < 1$. The equation of motion for a single particle without interactions nor collisions is then

$$\begin{cases} \frac{d\vec{v_p}}{dt} = \frac{1}{T_p}(\vec{u} - \vec{v_p}) \\ \frac{d\vec{x_p}}{dt} = \vec{v_p} \end{cases} \tag{17}$$

Note that the acceleration is expressed using the particle relaxation time

$$T_p = \frac{D_p^2}{18\nu} \tag{18}$$

and can be precomputed if one assumes the particles have constant mass, diameter, and density. Note that in Equation 17 the velocity field of the continuous phase (here: combustion gas) is a *continuous* field. An interpolation method is required (see 3.2).

2.2.2 Turbulence

To capture turbulence effects acting on the particles, the Reynolds decomposition is again used for the velocity, $\vec{u} = \vec{U} + \vec{u}'$. In theory, one may provide any mean velocity field $\vec{U}$, but in this project the mean field is set to $\vec{U} = [u_x(y), 0, 0]$, where $u_x(y)$ is the interpolated result from the finite-volume solution of (7). The fluctuations u' are calculated using the Langevin model using the turbulent scales.

The form of the Langevin model used in this project is taken from the lecture notes:

$$u'_{n+1} = u'_n e^{-\Delta t/T_L} + \sigma_{u'}\eta(0,1)\sqrt{1 - e^{-2\Delta t/T_L}} \tag{19}$$

This is a stochastic ODE. Here, T_L is the time in which the particle experiences the current eddy, and $\eta(0,1)$ is a standard Gaussian distribution. The parameter $\sigma_{u'}$ is derived from the turbulent kinetic energy. Assuming isotropic turbulence,

$$\sigma_{u'} = \sqrt{\frac{2}{3}k} = \frac{l_m}{T_t} = u' \tag{20}$$

and

$$T_t = \frac{1}{dU/dy} \tag{21}$$

3 Numerical method

We use the following cell indexing:

- P: Current cell centre
- N: North neighbour centre
- n: Shared cell face between P and N
- S: South neighbour centre
- s: Shared cell face between P and S

The top and bottom cells have their n and s faces coinciding with the top and bottom walls, respectively. To enforce boundary conditions on the top and bottom cells, ghost nodes are used. Each cell has width Δy_i, so the distance between P and N centres is $(\Delta y_P + \Delta y_N)/2$.

3.1 Mesh generation

A mesh is supplied to the routine as an input and may be generated using any appropriate method. In this project, three methods have been used:

- **Uniform meshes:** The number of cells are provided by the user.
- **Uniform core meshes:** The number of cells are provided by the user. Additionally, the user provides the distance between the first cell centre and the wall. The remaining vertical space will be distributed evenly for the remaining cells. This works well with wall functions.
- **Skewed mesh:** The number of cells are provided by the user together with a skew parameter. Increasing skew will place more cells closer to the walls. This works well for wall damping. An example is shown in Figure 6.

3.2 Numerical discretization

The integrated form of (7) is

$$\left(\mu \frac{du}{dy}\right)_n - \left(\mu \frac{du}{dy}\right)_s = \frac{dP}{dx} \Delta y_P \tag{22}$$

Here, μ is the total (effective) viscosity. The shear stress at the cell faces is not known, but may be estimated using the known viscosities at the cell centres by using an interpolation scheme. First, the face stresses are decomposed:

$$\mu_n \left(\frac{du}{dy}\right)_n - \mu_s \left(\frac{du}{dy}\right)_s = \frac{dP}{dx} \Delta y_P \tag{23}$$

The formula used for interpolating viscosity at the cell faces is the uneven two-point linear interpolation scheme. For the north face, this corresponds with

$$\mu_n = \left(1 - \frac{\Delta y_P}{\Delta y_P + \Delta y_N}\right)\mu_P + \frac{\Delta y_P}{\Delta y_P + \Delta y_N}\mu_N \tag{24}$$

which for $\Delta y_P = \Delta y_N$ reduces to

$$\mu_n = \frac{\mu_P + \mu_N}{2} \tag{25}$$

Central differencing is used to approximate the velocity gradient at the cell face:

$$\left(\frac{du}{dy}\right)_n \approx \frac{u_N - u_P}{(\Delta y_P + \Delta y_N)/2} \tag{26}$$

Similar formulations for viscosity and velocity gradients are made for the south face. This is all the discretization needed for the internal cells; special treatment to the boundary cells are required.

3.2.1 Prescribed slip velocity

The wall velocity is the average between the boundary cell and its ghost equivalent:

$$u_{\text{wall}} = \frac{u_P + u_{-P}}{2} \tag{27}$$

One can then rearrange for u_{-P} and insert this into the discrete equation for the boundary cell. This method also works for a no-slip condition.

3.2.2 Prescribed wall shear stress

If the shear stress at the wall is prescribed, the corresponding stress term in Equation 22 can just be substituted. For example, if τ_w is prescribed for the south wall, then

$$\mu_n \left(\frac{du}{dy}\right)_n - \tau_w = \frac{dP}{dx}\Delta y_P \tag{28}$$

When the linear system for u is built, the shear stress will appear on the right hand side as a source term.

3.3 Numerical solution scheme

In the previous section, it was assumed that the effective viscosity is known at the cell centres. For turbulent flow, the eddy viscosity is not known until the velocity field is also known. To solve this non-linear problem, a simple iterative scheme is used:

- Initialize the mesh with no turbulent viscosity $\mu_{\text{eff}} = \mu_{\text{mol}}$

- Solve the linear system to get an intermediate solution u^*
- Calculate the effective viscosity using u^* and possibly a relaxation parameter
- Repeat step 2 and 3 until convergence, indicated by $|u - u^*|_2 < \text{tol}$

The code has been verified by running a number of cases with varying mesh and boundary conditions. See Appendix.

3.4 Interpolation scheme for gas velocity field

The finite volume solution using wall functions is too coarse for particle tracking close to the wall. The velocity field is therefore resampled to a new mesh with a uniform distribution. For all positions further away from the wall than the boundary cell centres, linear interpolation is used. For positions closer to the wall than the boundary cell centres, the log law is used. Since the resampled mesh is uniform, fetching the gas velocity at any arbitrary particle position can be done in constant time complexity.

4 Results

A channel with $H = 0.1\,\mathrm{m}$ is simulated for a gas with $\rho = 1.5\,\mathrm{kg/m^3}$ and $\mu_{\mathrm{mol}} = 1.2 \times 10^{-4}\,\mathrm{Pa}$. The number of cells in the gas mesh is 201, while the number of cells in the resampling mesh is 1000. The particles have a diameter of $11.04\,\mu\mathrm{m}$ with a standard deviation $0.30\,\mu\mathrm{m}$ and density $\rho_p = 2300\,\mathrm{kg/m^3}$. 10,000 particles (parcels) are chosen to represent $2.5\,\mathrm{g/s}$ of SiO_2. With some rough estimations using the mean particle diameter, each parcel contains 10^5 particles.

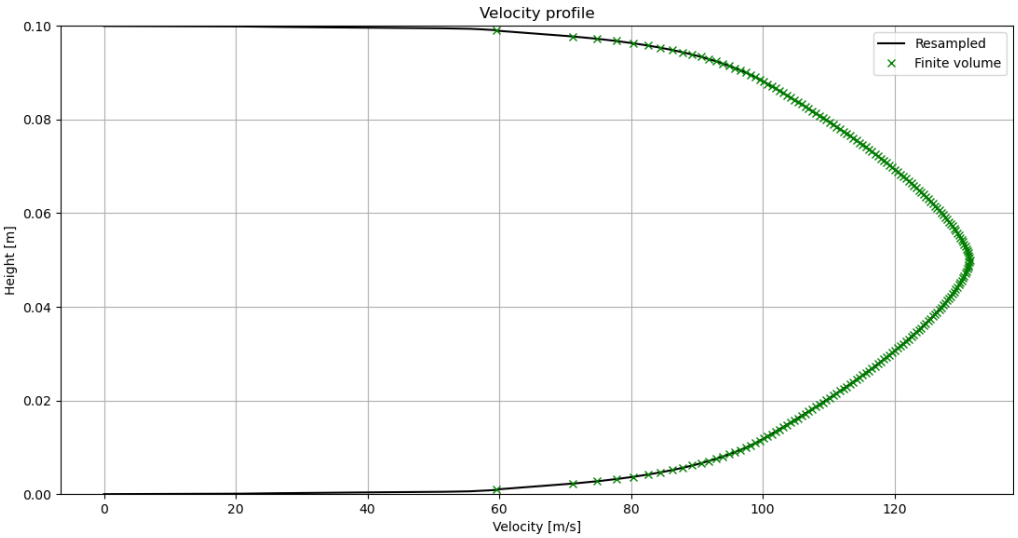

Figure 3: Gas velocity field for the final simulation case.

Figure 3 shows the gas velocity field which is found using the developed code. Wall functions are used. The compute time is less than 0.1 s.

The particles are tracked using a time step of $2 \times 10^{-6}\,\mathrm{s}$, which is smaller than T_t found using the mixing length model for the gas, such that the particle fluctuations will be captured properly. The channel is divided into 100 equally sized bins in the x-direction for mass tracking.

Figure 4 shows that simulating for about 0.2 s is long enough to reach steady deposition rates. After this, the mass in each bin is scaled up to correspond with a 10 s simulation time, which enables comparisons with the previously mentioned results from Copenhagen Suborbitals. This saves compute time.

The final deposit thickness is the correct order of magnitude. It is challenging to determine the accuracy of the simulation. There is a clear bias toward the channel inlet. This is most likely due to an unidentified mistake in the code. Far from the inlet, the thickness is $50\,\mu\mathrm{m}$, which is reasonable, but it is trending toward zero thickness.

While the gas field solution is simplified a lot from the real case, the method used captures the most important features of the flow field; the core velocity is high, and the

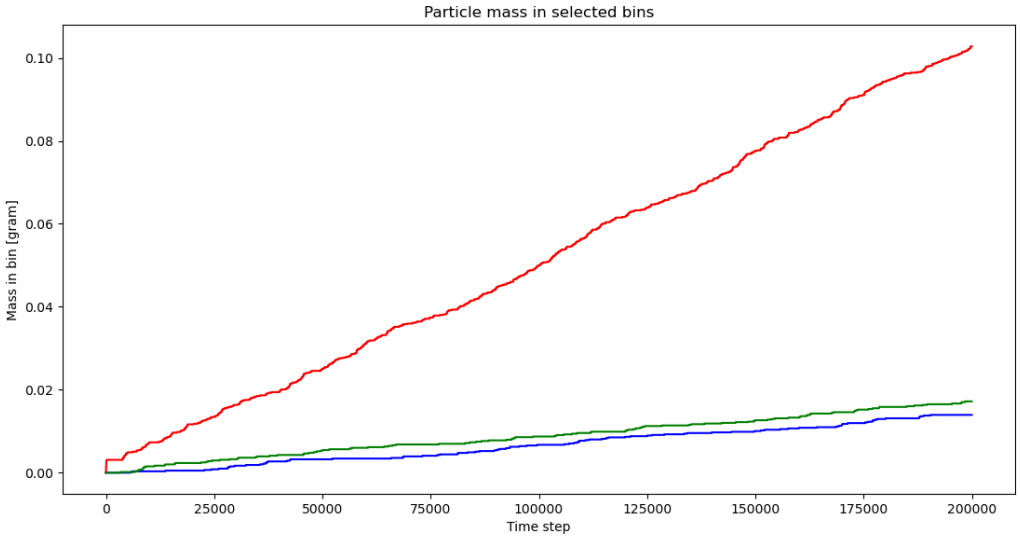

Figure 4: Deposition rates. Red line is bin 1/100, green line is bin 50/100, and blue line is bin 100/100.

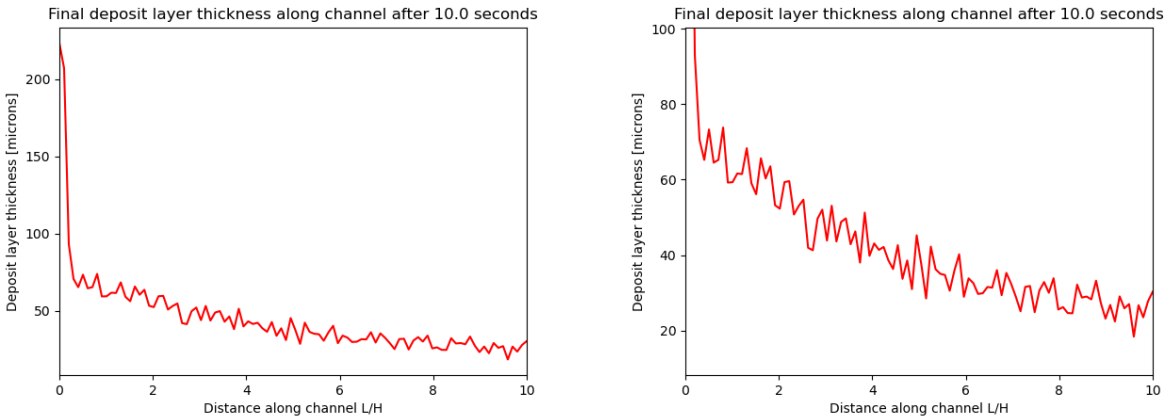

(a) Final deposit layer thickness along the channel.

(b) Zoomed-in view of the final deposit layer thickness.

Figure 5: Results of the particle tracking.

gradient towards the wall is very steep. The method used for the gas field is likely not to be contributing to the unusual deposit thickness distribution.

It has been confirmed that the particle Reynolds number is less than 1 (by a significant amount), meaning Stokes drag is an appropriate model to use.

References

[1] Tae Jun Jeon and Tae Seon Park. Thermal recycling analysis in regenerative cooling channels based on liquid rocket engine cycles. *Applied Thermal Engineering*, 256:124095, 2024.

[2] Ibrahim Chehimi, Jay Johal, and Sam Owen. Critical design review. *Internal Report*, April 2025. Team Name: UCL Rocket, Academic Year: 2024–2025.

[3] Thomas Pedersen. A few um of sio2, please!, June 2018. Published by Copenhagen Suborbitals. Photo by Carsten Olsen.

[4] K. Hanjalić, S. Kenjereš, M. J. Tummers, and H. J.J. Jonker. *Analysis and Modelling of Physical Transport Phenomena*. VSSD, Delft, The Netherlands, 1st, corrected 2009 edition, 2007. Department of Multi-Scale Physics, Faculty of Applied Sciences, Delft University of Technology.

A Verification

A.1 Single phase flow

The single phase flow solver is tested independently of the particle tracking.

A.1.1 Laminar flow

The implementation of the linear solver for single phase flow is verified by prescribing the pressure gradient and channel height with different boundary conditions.

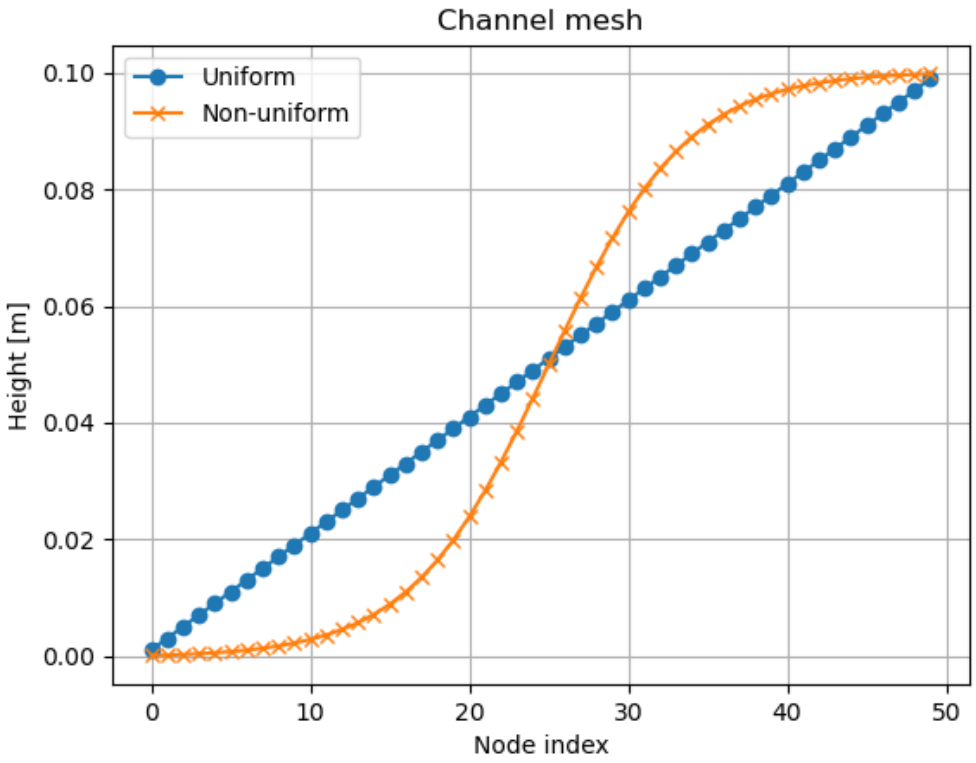

Figure 6: Mesh used for verification of implementation.

All results are satisfactory.

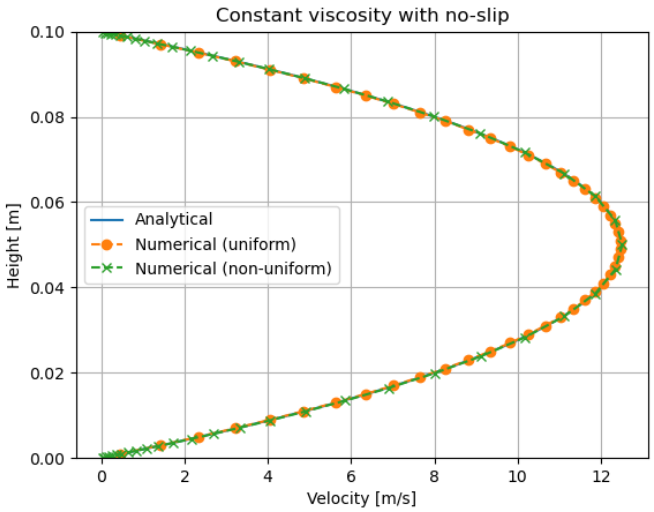

Figure 7: Laminar results with no-slip conditions and prescribed pressure gradient. Numerical results coincide with analytical formula.

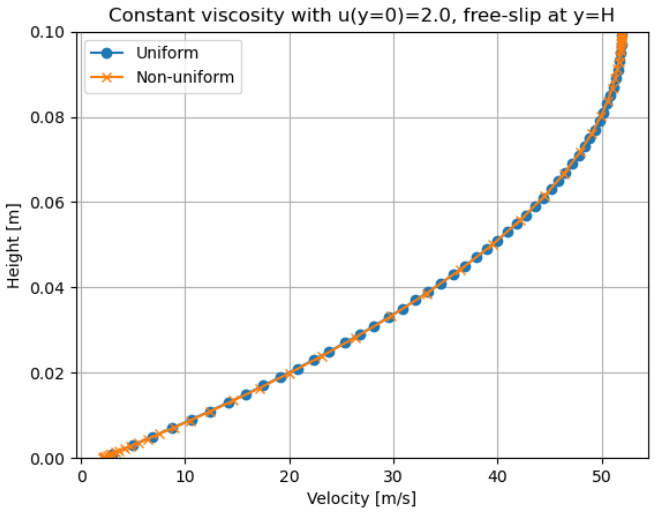

Figure 8: Laminar results with mixed wall boundary conditions.

A.1.2 Turbulent flow

For turbulent flow, the mesh is adapted to reach a target y^+ value, as described in the main section of this report.

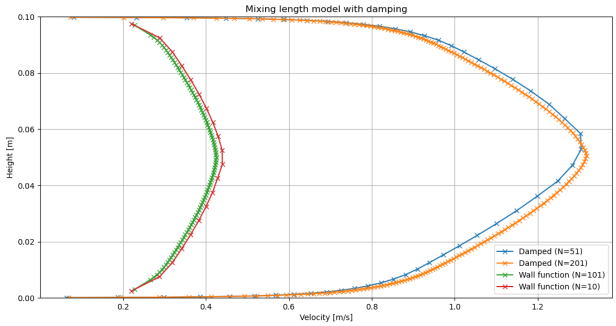

Figure 9: Velocity results for four different meshes using wall damping or wall functions.

Figure 9 shows inconsistencies between the two wall treatments. The wall damping methods is likely most similar to DNS results. Wall function results may be incorrect due to the discretization method. There was not enough time to investigate this further.

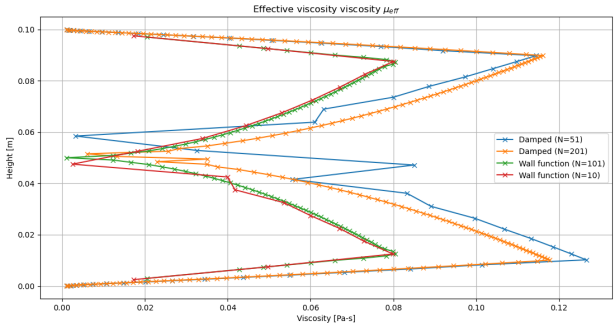

Figure 10: Total viscosity in the channel. Molecular viscosity is $\mu_{\text{mol}} = 10^{-3}$.

The results may be plotted in wall units by normalizing by u_τ where u_τ is calculated from the prescribed pressure gradient. This result is shown in Figure 11 together with the law of the wall (purple).

The results using wall functions are satisfactory, and this wall treatment will be preferred over wall damping going forward.

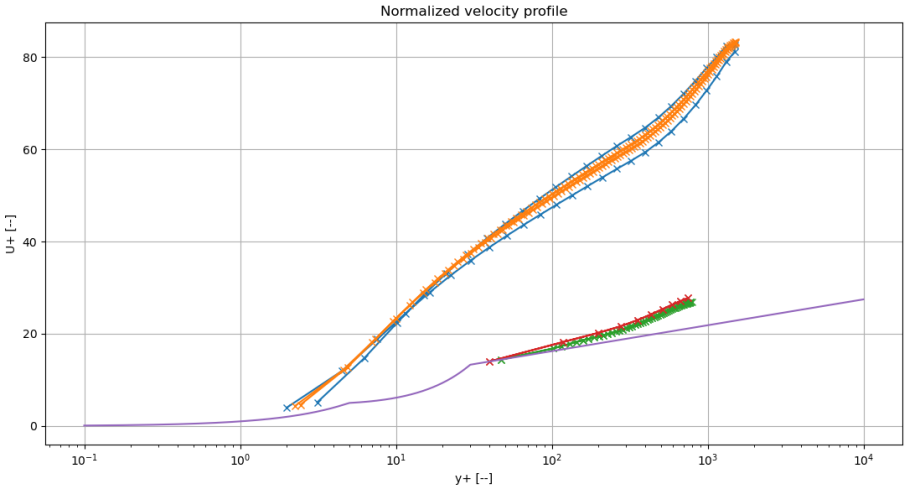

Figure 11: Comparison between different results in wall units, using u_τ calculated from dP/dx. The coloring is the same as the two previous figures.

A.2 Particle-laden flow

For the verification of the particle tracking implementation, larger particles have been used (1 mm).

A.2.1 Single particle

The particle tracking is first validated using a uniform gas field, $\vec{u} = (1, 0, 0)$ with no turbulence. A single particle is initiated at the centre of the channel with a high enough y-velocity to hit the wall at least once.

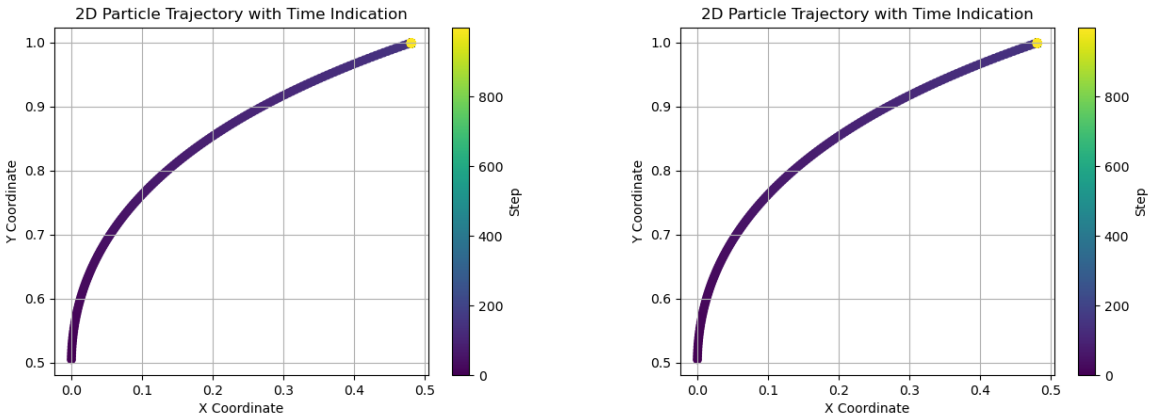

(a) Tracking of a single particle with absorbing walls.

(b) Tracking of a single particle with absorbing walls. Note the periodic boundary condition in the x-direction.

Figure 12: Test of particle tracking in a uniform gas field.

The results are satisfactory.

A.2.2 Multiple particles

Particles are placed at $x = 0$ at $t = 0$ with no initial velocity in a gas field, and the location is tracked.

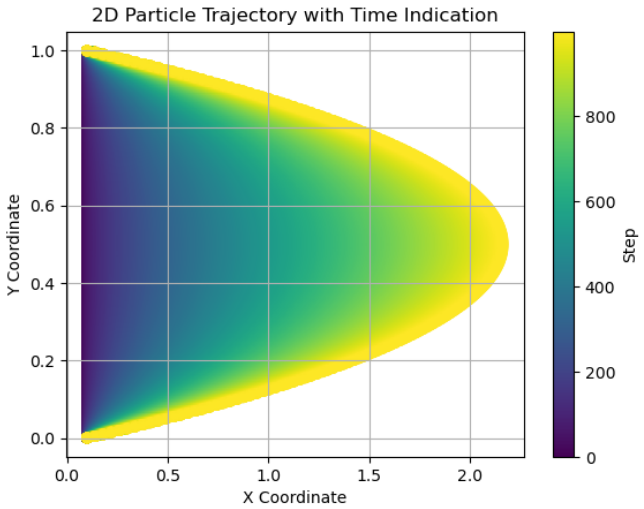

Figure 13: Particle tracking with laminar (parabolic) gas flow field.

The behaviour with laminar gas field is as expected; particles in the centre of the channel accelerate more than the particles closer to the wall. The parabolic shape is observable through the particle front.

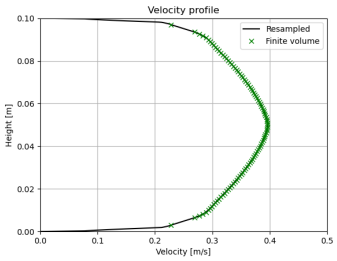

(a) Velocity resampling for the turbulent test case.

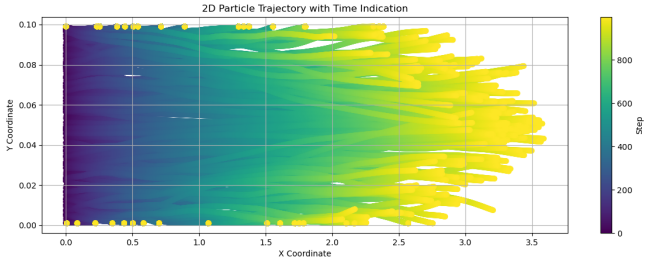

(b) Traces of multiple particles in a turbulent gas field.

Figure 14: Test of particle tracking with turbulence. The wall is absorbing and all particles are initiated at $t = 0$.

All results are satisfactory.

B Code

The source code for this project is 2500 lines and is therefore not included here. The codebase is publicly available from 01. August 2025 on GitHub:
willidu/AP3551-Multiphase-Flow.
The main code can be found in `homework/src/steady_single_phase.cpp` and in `homework/src/particle_tracking.cpp`.